Environmental Science
Processes & Impacts

Incorporating Concentration-Dependent Sediment Microbial Activity into Methylmercury Production Kinetics Modeling

Journal:	*Environmental Science: Processes & Impacts*
Manuscript ID	EM-ART-07-2021-000287.R1
Article Type:	Paper

Environmental Significance Statement (120wds)

Traditional kinetic models for predicting methylmercury (MMHg) production in sediments assume mercury (Hg) and MMHg are fully available for methylation and demethylation processes. A transient availability model (TAM) for MMHg production kinetics incorporates terms for processes, such as adsorption, that impact the availability of Hg and MMHg to participate in methylation and demethylation reactions. This work tests the applicability of the TAM on MMHg production in sediments. Results show that the TAM is generally applicable to sediments but is more accurate in predicting MMHg production in organic-poor sediments. To improve the model fit in organic-rich, microbially active sediments, a Monod kinetics term was added to the TAM to account for concentration-dependent microbial activity during the MMHg production experiments.

Incorporating Concentration-Dependent Sediment Microbial Activity into Methylmercury Production Kinetics Modeling

Grace E. Schwartz,[a,†] Katherine A. Muller,[b] Saubhagya S. Rathore[a], Regina L. Wilpiszeski,[c] Alyssa A. Carrell,[c] Melissa A. Cregger,[c] Dwayne A. Elias,[c] Mircea Podar,[c] Scott L. Painter[a], Scott C. Brooks[a, *]

[a]Environmental Sciences Division, Oak Ridge National Laboratory, P.O. Box 2008, MS 6038, Oak Ridge, Tennessee 37831-6038

[b]Earth Systems Science Division, Pacific Northwest National Laboratory, Richland, WA

[c]Biosciences Division, Oak Ridge National Laboratory, P.O. Box 2008, MS 6038, Oak Ridge, Tennessee 37831-6038

[†]Current Affiliation: Department of Chemistry, Wofford College, 429 N. Church St, Spartanburg, SC 29303

[*]Corresponding Author: Email: brookssc@ornl.gov, Phone: 865-574-6398, Fax: 865-576-8646.

Keywords: methylmercury, kinetics, sediment, Monod, transient availability

Abstract

In anoxic environments, anaerobic microorganisms carrying the *hgcAB* gene cluster can mediate the transformation of inorganic mercury (Hg(II)) to monomethylmercury (MMHg). The kinetics of Hg(II) transformation to MMHg in periphyton from East Fork Poplar Creek (EFPC) in Oak Ridge, TN have previously been modeled using a transient availability model (TAM). The TAM for Hg(II) methylation combines methylation/demethylation kinetics with kinetic expressions for processes that decrease Hg(II) and MMHg availability for methylation and demethylation (multisite sorption of Hg(II) and MMHg, Hg(II) reduction/Hg(0) oxidation). In this study, the TAM is used for the first time to describe MMHg production in sediment. We assessed MMHg production in sediment microcosms using two different sediment types from EFPC: a relatively anoxic, carbon-rich sediment with higher microbial activity (higher CO_2 production from sediment) and a relatively oxic, sandy, carbon-poor sediment with lower microbial activity (lower CO_2 production from sediment). Based on 16s rRNA sequencing, the overall microbial community structure in the two sediments was retained during the incubations. However, the *hgcA* containing methanogenic *Euryarchaeota* communities differed between sediment types and their growth followed different trajectories over the course of incubations, potentially contributing to the distinct patterns of MMHg production observed. The general TAM paradigm performed well in describing MMHg production in the sediments. However, the MMHg production and ancillary data suggested the need to revise the model structure to incorporate terms for concentration-dependent microbial activity over the course of the incubations. We modified the TAM to include Monod-type kinetics for methylation and demethylation and observed an improved fit for the carbon-rich, microbially active sediment. Overall our work shows that the TAM can be applied to describe Hg(II) methylation in sediments and that

including expressions accounting for concentration-dependent microbial activity can improve the accuracy of the model description of the data in some cases.

1. INTRODUCTION

Mercury (Hg) is a trace metal pollutant that enters the environment from both natural and anthropogenic sources. While the majority of the Hg released into the environment is in the form of inorganic Hg, either as Hg(0) or Hg(II), the organic Hg form of monomethylmercury (MMHg) presents the greatest threat to human health [1]. MMHg is a central nervous system toxin [2] that biomagnifies in the food web [3] and poses a health risk, particularly for developing fetuses and young children. MMHg is formed from Hg(II) in a process carried out by anaerobic microorganisms containing the *hgcAB* gene cluster [4]. The amount of MMHg produced in an ecosystem depends on a complex array of factors, including the identity and activity of the methylating microbial community, the availability of Hg(II) for methylation, and the rate of MMHg degradation [5, 6]. MMHg production has been observed in many different environments, including anoxic sediments, anoxic microenvironments in biofilms, and on particles in the water column [5, 7]

Predicting the net MMHg production potential of an environment is useful for assessing MMHg risk and formulating MMHg remediation solutions. The method of choice for assessing MMHg production potential is to use stable isotope tracers ($HgCl_2$ and MMHgCl) to track methylation and demethylation reactions in environmental samples. The added tracers are generally thought to be more biologically available than ambient Hg and MMHg [8], and may overestimate methylation and demethylation rates. However, especially in contaminated systems, isotope tracers are a valuable tool that can give a reasonable estimation of methylation and demethylation in the environment. Rate constants derived from isotope tracer experiments are referred to as rate potentials, acknowledging that they may not exactly mimic ambient Hg(II) and

MMHg behavior. In one method, the stable isotopes are injected into intact sediment cores to measure methylation and demethylation at a single time point [9, 10]. This method is perhaps the closest to measuring methylation and demethylation in situ, but it is difficult to evenly distribute the isotope spikes and heterogeneity within the core often leads to noisy data. In another approach, isotope tracers are spiked into microcosms or mesocosms containing homogenized sediment to obtain methylation and demethylation rates over a time course [11-14]. The latter design tends to provide better quality data and a more complete picture of methylation and demethylation rates. However, in some instances, homogenization of the sediment and carbon and nutrient limitations in the microcosms make it difficult to exactly mimic in situ conditions.

Isotope tracer methylation and demethylation data have traditionally been described using a first-order reversible kinetic model that assumes full availability of Hg(II) and MMHg for methylation and demethylation reactions [9]. However, time series methylation/demethylation data often display apparent non-first order kinetic behavior [13, 14], making first-order rate potentials difficult to interpret. Recently, a transient availability kinetic model (TAM) was developed for net MMHg production in periphyton biofilms to fit this apparent non-first order behavior [15]. The TAM accounts for competing processes that may reduce Hg(II) and MMHg availability for methylation and demethylation, respectively, by combining kinetic expressions for multisite sorption of Hg(II) and MMHg, Hg(II) reduction/Hg(0) oxidation, and methylation/demethylation kinetics [15]. Initial work with the TAM shows a better fit to time course MMHg production in periphyton compared to full availability, single time point kinetics [15, 16]. However, it is unclear if the same TAM can be applied to MMHg production in other matrices, such as sediments, if changes to the model structure within the same paradigm are needed, or if a new model paradigm is required. Aquatic sediments represent a major source of

MMHg to the environment. Though many of the broad parameters that control methylation in periphyton will also impact methylation in sediment (e.g., redox potential and the activity of Hg-methylating microorganisms), aquatic sediments present a very different habitat with unique and complex biogeochemistry that could greatly impact methylation kinetics.

Sediment biogeochemistry touches every aspect of Hg(II) methylation, including Hg-methylator identity and activity, Hg(II) bioavailability, and MMHg degradation. The microbial community and redox potential of an ecosystem are shaped by the relative prevalence of different electron acceptors [5]. The types and concentrations of organic carbon substrates and their accessibility to microorganisms impacts the overall microbial diversity and activity, including that of MMHg-producing microorganisms [5, 17, 18]. Hg(II) speciation and bioavailability to Hg-methylating bacteria is largely governed by the relative concentrations and complex interplay of sulfide and DOM [19]. High sulfide concentrations may limit Hg bioavailability due to the precipitation of $HgS_{(s)}$, though some high sulfide environments have shown enhanced methylation [20]. DOM increases the dissolution rate of $HgS_{(s)}$ [21] and can also inhibit the aggregation and precipitation of $HgS_{(s)}$ from solution, increasing bioavailability to methylating microorganisms.[22] [23-25]. In sulfidic conditions, organic matter is increasingly sulfurized, enhancing Hg(II) complexation with dissolved organic matter and overall Hg(II) bioavailability [26]. The ratio of reduced Fe to reduced S can have an indirect effect on Hg(II) speciation by precipitating reduced sulfur from solution, affecting the amount of reduced sulfur available to complex with Hg(II) in solution, or in some instances, forming FeS-DOM colloids that stay in solution and enhance DOM complexation with Hg(II) and Hg(II) bioavailability [27]. The presence of reduced sulfur surfaces, such as mackinawite (FeS), can also catalyze demethylation reactions [28, 29].

The previously developed TAM accounts for changing Hg(II) and MMHg concentration over time with rate constants derived from Hg(II) and MMHg adsorption reactions [15]. Here we test whether the current form of the model is applicable under the added complexity of sediment systems. To develop a transient availability kinetic model for sediments, it is imperative to consider the heterogeneity of sediment types. In this study, we apply the TAM to two distinct sediments from East Fork Poplar Creek (EFPC) in Oak Ridge, TN, USA, which is contaminated with Hg from cold-war era industrial activity [30]. Here we characterize the physical, chemical, and microbial characteristics of the two types of sediment, measure MMHg production/degradation, as well Hg(II) and MMHg sorption, and Hg(0) formation. The objective of this work was to produce a TAM of MMHg production applicable to sediments, with the future goal of integrating the results into a field-scale model of EFPC to predict MMHg fluxes within the watershed.

2. MATERIALS AND METHODS

Previous studies give a detailed history and characterization of EFPC [30, 31]. Briefly, EFPC is a low-order stream in east Tennessee, USA with a history of Hg contamination dating back to the 1950's. The creek meanders 26 kilometers from its headwaters in an industrial complex through urban, suburban, and forested sections of its watershed to the confluence with Poplar Creek.

2.1 Sediment collection and characterization. Sediment cores (n=12) were collected from EFPC kilometer 5.4 on 7/17/18 for Sediment 1 and on 8/28/18 for Sediment 2. Sediment 1 is finer grained and is prevalent on the margins of EFPC, where tree roots, submerged wood, rocks, and other obstructions slow water movement. Sediment 1 is carbon-rich and more anoxic compared to Sediment 2. Sediment 2 predominates in the main channel of the creek and on

sandbars throughout the creek. It is made up of a medium to coarse sand that is low in organic carbon and has a generally higher redox potential. Water residence times are greater in Sediment 1 than in Sediment 2 leading to the development of deeper and more highly reducing conditions in areas dominated by Sediment 1.

Cores were collected by hand using 25 cm long x 4.8 cm diameter clear polycarbonate tubes, and the sediment cores ranged from 10 to 16 cm in depth. The cores were stored upright after collection and immediately transported back to the laboratory (20 minutes). Upon arrival at the laboratory, the cores were transferred into an anaerobic chamber (Coy Labs) with a 98%N_2/2% H_2 atmosphere where they were combined into a large bowl and gently homogenized by hand with a trowel. The bulk sediments were characterized by measuring (Table 1; Analytical Methods and SI): percent water content, loss on ignition (%LOI) as an estimate of natural organic matter concentration, Brunauer-Emmet-Teller (BET) surface area, grain size distribution, acid-extractable total Fe and Fe(II) concentrations, ambient Hg(II) and MMHg concentrations, and CO_2 and CH_4 generation. These methods are detailed in the Supporting Information section. A subsample of the homogenized sediments was preserved at -80°C for molecular microbial characterization.

2.2 MMHg and Hg(II) Adsorption Experiments. Hg(II) and MMHg adsorption experiments were used to monitor the time-dependent partitioning of added Hg(II) (^{201}Hg) and MMHg (MM^{202}Hg) isotope tracers between the dissolved and solid phases. The isotopes (^{201}Hg , 96.17% purity; ^{202}Hg, 95.86% purity) were purchased from Oak Ridge National Laboratory. MM^{202}Hg was synthesized in-house using the methylcobalamin method [32]. The adsorption experiments were conducted on the 0.149 mm to 0.5 mm size fraction of the dry, sieved, sediments (surface area shown in Table 1). EFPC surface water was collected from EFPC

kilometer 5.4 and filtered through a 0.2 μm polyethersulfone (PES) membrane flow-through filter prior to use in the experiments. Average water quality parameters are described in Table S1. Triplicate samples were prepared for all time points using 0.25 ± 0.01 g sediment, 20 mL of creek water in trace-metal clean clear glass vials for Hg(II) experiments, and 25 mL creek water in trace-metal clean amber for MMHg experiments.

In the Hg(II) adsorption experiments, dissolved Hg(II), solid-phase Hg(II), and Hg(0) were all quantified. The surface water was spiked with ^{201}Hg in the form of ^{201}HgCl at ~28% of the ambient Hg(II) content of the sediment (538 ng for Sediment 1, 1049 ng for Sediment 2). The spiked solutions were gently mixed on a rotating shaker at 100 RPM at room temperature for at least 1h. After 1h, 0.25 ± 0.01g of the dried sediment was added to the spiked solution, which was shaken vigorously by hand and then placed back on the rotating shaker for the incubation period. At each timepoint, the sample solution was vacuum filtered through a 0.2 μm PES filter unit (Nalgene). A 100 μL aliquot of the filtrate was transferred to 20 mL of Milli-Q water. This sample was then purged with high purity N_2 for 10 min at 30 PSI to collect Hg(0) onto a gold trap. The remaining filtrate was preserved with trace metal grade concentrated HCl at 0.5% (v/v) and stored at 4°C. The filter was cut out of the filter unit and placed in the sample vial with the residual solids. These solids were digested with aqua regia and prepared for analysis as described below. Samples were taken at regular intervals between 1 and 1800 minutes for Sediment 1, and at 1 and 2880 minutes for Sediment 2. Mass balance recoveries averaged 97.8 ± 3.6 for Sediment 1 and 93.6 ± 5.7 % for Sediment 2. Control samples without sediment were prepared and analyzed at 10 and 1800 min, with mass balance recovery of the ^{201}Hg of 92.0 ± 0.4 and 82.7 ± 1.3%, respectively.

For the MMHg adsorption experiments, $MM^{202}Hg$ in the form of $MM^{202}HgCl$ was spiked into the surface water at ~190% of the ambient MMHg (4.08 ng for Sediment 1, 0.68ng for Sediment 2). This spike level was chosen to ensure that $MM^{202}Hg$ could still be quantified in the aqueous phase, even if 90% or more sorption occurred. The spiked solution was gently mixed on a rotating shaker at 100 RPM for at least 1h. After 1h, 0.25 ± 0.01g of the dried sediment was added to the $MM^{202}Hg$-spiked water. The samples were mixed vigorously by hand and then placed back on the rotary shaker for the designated incubation period. Samples were taken at regular intervals between 5 and 1800 minutes for both sediments. At each timepoint, the samples were taken off the shaker and filtered through a 0.2 μm PES syringe filter. The filtrate was preserved at 0.5% (v/v) with trace metal grade concentrated HCl and stored at 4°C until analysis. The solid phase was analyzed on a selection of samples to calculate the mass balance of the $MM^{202}Hg$ spike. Mass balance recovery (mass recovered from the filtrate + mass recovered from the solid) averaged 77.7 ± 1.5% for Sediment 1 and 88.0 ± 3.5% for Sediment 2. These mass balances likely reflect some loss of sediment-associated $MM^{202}Hg$ to the syringe filter, which was not extracted and the additive effect of some incomplete extraction of MMHg during two separate distillation and analyses. To determine if there was any loss of $MM^{202}Hg$ due to demethylation, "Whole slurry" samples were prepared and analyzed both at room temperature and at 4°C. The whole slurry samples were prepared as described above, but they were not filtered at the timepoint. Rather, the entire sample was preserved with HCl and placed at 4°C until analysis. The entire slurry sample was then distilled and analyzed for MMHg. $MM^{202}Hg$ spike recovery was nearly identical in the 4°C and room temperature slurries (94.7 ± 1.8% and 94.3 ± 3.3%, respectively), giving no evidence of biotic demethylation or substantial abiotic demethylation. Control samples without sediment were also prepared and analyzed at 20m, 2h,

and 12h, and mass balances for the $MM^{202}Hg$ spike were 93.7 ± 0.6, 102 ± 3% and 107 ± 2%, respectively.

2.3 Hg(II) Methylation-MMHg Demethylation Experiments.

2.3.1 Experiment design. Sediment slurry microcosm experiments were conducted to determine the Hg(II) methylation and MMHg demethylation potentials of Sediment 1 and Sediment 2. Three types of microcosms were constructed: methylation microcosms spiked with ^{201}Hg to monitor the production of $MM^{201}Hg$, microcosms spike with $MM^{202}Hg$ to monitor demethylation, and control microcosms with no Hg/MMHg spike that were set up in parallel to track geochemical parameters throughout the experiment. A subset of the control microcosms was designated for microbial diversity analyses at the final incubation timepoint. Microcosms were prepared in triplicate and sacrificed at each timepoint. The Sediment 1 experiment had five time points: 0d, 1d, 2d, 3d, and 4d. The Sediment 2 experiment had four time points, but due to lower microbial activity conditions in the microcosms, we allowed the experiment to run longer with time points at 0d, 3d, 10d, and 14d.

2.3.2 Microcosm Preparation. For both experiments, EFPC surface water was vacuum filtered through a 0.45 μm glass fiber filter to remove sediment particles. The surface water was then amended with resazurin (6 mL of 0.1% (w/v) resazurin to 1000mL water). Resazurin is a redox indicator that that turns from pink to clear when reduced (midpoint potential -50mV). The surface water was sparged with N_2 for at least 30 min and then moved to the anaerobic chamber. The homogenized sediment was weighed out (10 g ± 0.5 g) into serum bottles and 20 mL of the resazurin-surface water mixture was added to each serum bottle. Sediment 1 microcosms were capped in the anaerobic chamber with butyl rubber stoppers and aluminum crimp caps, removed from the chamber, and purged with high-purity N_2 for 5 min. The microcosms were returned to

the anaerobic chamber, and the appropriate bottles were spiked with $^{201}HgCl_2$ (6.6 μg for Sediment 1, 13.1 μg for Sediment 2) to monitor methylation or $MM^{202}HgCl$ (28.0 ng for both sediments) to monitor demethylation. The Sediment 1 microcosms were spiked the same day of the sediment collection, immediately after the purging step. The Sediment 2 microcosms were held in the anaerobic chamber overnight after the purging step and were spiked the morning of the next day.

2.3.3 Microcosm deconstruction and sampling. At each timepoint, methylation and demethylation microcosms were acidified with 10 mL of 18% (w/v) KBr/5% (v/v) H_2SO_4 and 2 mL of 1M $CuSO_4$ and the isotope dilution spike ($MM^{200}HgCl$) for MMHg analysis was added to each microcosm. The preserved microcosm samples were stored at 4°C until extraction and distillation for MMHg analysis. The geochemical control microcosms were also deconstructed at each time point. The supernatant of those microcosms was syringe-filtered through a 0.2 μm PES membrane and aliquoted for different analyses, including pH, dissolved organic carbon (DOC), anions, sulfide, Total Fe, and Fe(II) (methods described in the SI section). DOC samples were preserved with trace metal grade HCl at 0.1% v/v, stored at 4°C, and analyzed as mg C□L on a Shimadzu TOC-L. Anion samples were stored at -20°C until analysis on a Dionex ICS-2100 with an IonPac AS9-HC column. Samples for sulfide analysis were with mixed 1:1 with sulfur antioxidant buffer (2 M NaOH/0.2 M Sodium EDTA/0.2 M Ascorbic Acid) and analyzed within 6 h of collection via anion-specific electrode calibrated with Pb-titrated standards [33]. Aliquots for Fe were preserved at 1% HCl (v/v) and were stored at 4°C until analysis via ferrozine colorimetric assay via a modified version of the Stookey method (details are given in the SI)[34].

2.4 Analytical methods. For the MMHg production experiments, MMHg slurry sediments were prepared via total digestion and extraction following the Bloom et al. method [35]. The

extracted sample was then distilled following EPA Method 1630 [36] and analyzed via Isotope Dilution-Gas Chromatography-Inductively Coupled-Mass Spectrometery (ID-GC-ICP-MS). Solid phase samples and whole slurry samples from the MMHg adsorption experiments were directly distilled and analyzed via ID-GC-ICP-MS. Solid phase THg samples were digested in aqua regia (10 mL conc HCl:3 mL conc HNO_3) overnight, diluted to 40 mL with Milli-Q water, filtered through a 0.2 μm PES syringe filter, and diluted with Milli-Q water for analysis. The digests were then analyzed according to EPA Method 1631 and analyzed via ID-GC-ICP-MS [37]. For Hg(0) measurements in the adsorption experiments, the Hg(0) was thermally desorbed from the gold trap it was collected on and analyzed using a Brooks Rand Thermal Desorption unit coupled with an ICP-MS. Details of the other analytical methods are provided in Supporting Information.

2.5 Microbial Analyses. Aliquots of the initial sediment and control microcosms from the final incubation timepoints were frozen at -80°C for microbiological sequencing.

DNA extraction and sequencing. DNA was extracted from each sediment using the DNeasy PowerSoil Kit (Qiagen) following the standard protocol. Amplification and sequencing of the 16S rRNA gene was performed following the method of Lundberg et al, 2013[38] with modifications as described in Liang et al, 2018[39] using primers 515F and 806R (IDT). Amplification and high-throughput sequencing of the Hg(II) methylation genes *hgcAB* was performed using primers ORNL-HgcAB-uni-F and ORNL-HgcAB-uni-32R containing 5' Illumina sequencing adapters as described in Gionfriddo et al (2020)[40]. Amplicon pools were gel purified on a 1.5% agarose gel and cleaned using the Wizard SV Gel and PCR clean-up system (Promega) prior to sequencing. Second-round amplification for barcoding with the Nextera DNA

Library Preparation Kit (Illumina) and sequencing on the Illumina MiSeq v3 PE300 were performed at the University of Minnesota Genomics Facility (UMGC).

Sequence analysis. Sample processing for 16S community analyses were conducted in QIIME 2 v 2019.10 [41]. Sequences were trimmed, denoised, and error-corrected using DADA2 [42]. Representative sequences were classified against the Silva database v 132 [43] using the q2-feature-classifier plugin [44].

The forward-direction *hgcA* sequences were analyzed as described in Gionfriddo et al (2020)[40]. Briefly, sequences were filtered and trimmed to 201 base pairs using Trimmomatic [45]. Sequences were dereplicated, and singletons and chimeras were removed using USEARCH and VSEARCH [46]. OTUs were generated by clustering sequences at 90% similarity. Centroid sequences were assigned taxonomy using the reference package ORNL_HgcA_201.refpkg [47]. Downstream analyses were performed in R using the packages phyloseq and ggplot2 [48, 49].

2.6 Kinetic Modeling

The TAM developed by Olsen et al (2018) was used to calculate methylation and demethylation rate potentials [15]. The model assumes that dissolved Hg(II) and MMHg are available to microorganisms for methylation and demethylation, respectively. In our data collection, the filter-passing Hg(II) and MMHg serve as proxy measures of the dissolved concentrations. The transient availability model is described by Equations 1 and 2,

(1) $\frac{d[Hg]}{dt} = -k_m[Hg] + k_d[MMHg] - k_1[Hg] + k_2[Hg_f] - k_3[Hg] + k_4[Hg_s] - k_5[Hg] + k_6[Hg^0]$

(2) $\frac{d[MMHg]}{dt} = k_m[Hg] - k_d[MMHg] - k_7[MMHg] + k_8[MMHg_f] - k_9[MMHg] + k_{10}[MMHg_s]$

Where k_m is the methylation rate constant, k_d is the demethylation rate constant, k_1 is the Hg(II) fast site sorption rate constant, k_2 is the Hg(II) fast site desorption rate constant, k_3 is the Hg(II)

slow site adsorption rate constant, k_4 is the Hg(II) slow site desorption rate constant, k_5 is the rate constant for the conversion of Hg(II) to Hg^0, k_6 is the rate constant for the conversion of Hg^0 to Hg(II), Hg_f is the amount of Hg(II) sorbed to fast sorption sites, Hg_s is the amount of Hg(II) sorbed to slow sorption sites, k_7 is the MMHg fast site adsorption rate constant, k_8 is the MMHg fast desorption rate constant, k_9 is the MMHg slow adsorption rate constant, $MMHg_f$ is the amount of MMHg sorbed to fast sites, and $MMHg_s$ is the amount of MMHg sorbed to slow sites.

The model was fit to the data as described in Olsen et al. (2018) using the ordinary differential equation solver ode45 in MATLAB R2016a (The MathWorks) and the nonlinear fitting routine nlinfit which reports the parameter covariance matrix (used in uncertainty assessment) as part of the output. The fits were weighted by the standard deviation of each data set. Briefly, k_1-k_{10} were estimated by fitting the model, without the methylation-demethylation terms, to the Hg(II) and MMHg sorption data. Those sorption rate constants were held fixed in the full TAM (Eqns 1 and 2) which was fit to the $MM^{201}Hg$ and $MM^{202}Hg$ data sets by adjusting the values of k_m and k_d. Uncertainty in the model predictions was assessed using Monte Carlo simulations (n = 5,000) in which k_{1-10} and k_m and k_d were randomly sampled from a multivariate normal distribution based on the fitted parameters and their corresponding covariance matrices.

3. RESULTS AND DISCUSSION

3.1 Sediment Biogeochemistry. Sediment 1 was richer in organic matter and more metabolically active than Sediment 2 (Table 1 and Figure S2). Both sediments were classified as sand by particle distribution analysis (Figure S1; Tables S2, S3). However, Sediment 1 was majority fine sand and had a higher BET surface area than Sediment 2, which was majority medium to coarse-grained sand. The % LOI of Sediment 1 was 7.0% compared to 1.4% in

Sediment 2. In gas generation incubations, Sediment 1 generated an average of 4 times the CO_2 and 27 times the CH_4 as Sediment 2 at 72 hours (Figure S2). The ambient MMHg concentration of Sediment 1 was 6 times the concentration of Sediment 2, indicating that Sediment 1 provides a more conducive environment for MMHg production and accumulation (Table 1).

At phylum level, overall microbial community composition was similar between the two sediment samples with *Proteobacteria* being dominant in both sediments, with lower representations of *Bacteroidetes*, *Acidobacteria*, *Actinobacteria*, *Chloroflexi*, *Planctomycetes*, *Spirochetes*, and various Archaea. A large diversity of much less abundant other phyla was also detected (Figure S3). These results are similar to communities described in previous studies of EFPC [18, 50]. The methylating community identified by sequencing of the *hgcA* gene was similar to the overall community but much less diverse (Figure S4), which is expected since the *hgcAB* gene pair is found in a limited number of anaerobic Bacteria and Archaea. The most abundant *hgcA* sequences clustered with *Proteobacteria*, particularly *Deltaproteobacteria*, followed by *Chloroflexi*, *Euryarchaeota*, and *Spirochetes* in Sediment 1 and *Chloroflexi*, *Firmicutes*, and *Euryarchaeota* in Sediment 2 (Figure 3).

3.2 Hg(II) and MMHg Sorption. For both sediments, Hg(II) exhibited the same two scale, fast and slow, sorption behavior observed with Hg(II) and MMHg sorption to periphyton (Figure 1) [15] and cation metal sorption to sediments and colloids [51, 52]. For both sediments, there was an initial fast sorption phase followed by a slower sorption phase. Within 1 min, 20% and 15% of the ^{201}Hg spike had adsorbed to Sediment 1 and Sediment 2, respectively (Figure 1). Dissolved Hg(II) continued to decrease over time. By 1d, 96.3% ± 1.8% of the ^{201}Hg spike had sorbed to Sediment 1. Overall, there was less sorption to Sediment 2 with 56.7% ± 1.6% of the ^{201}Hg spike sorbed at 1d. Hg(0) production never exceeded 3% for Sediment 1 and 5% for Sediment 2 (with

the exception of one data point at 0.25 d) across the entire experiment. The Hg(II) sorption data onto both sediments was described well by the two-site reversible kinetic sorption model embedded within the TAM (Figure 1, Table 2).

The MMHg sorption data were also well described by with the two-site sorption model (Figure 2; Table 2). However, the MMHg sorption behavior of the two sediments was markedly different. For Sediment 1, the proportion of the $MM^{202}Hg$ spike sorbed increased from 15.3% ± 0.3% at 5 min to 91.2% ± 0.3% at 1d. Sorption to Sediment 2 still displayed two-site sorption behavior, but the proportion of $MM^{202}Hg$ sorbed was much less compared to Sediment 1. $MM^{202}Hg$ sorption increased from 7.7% ± 1.1% at 5 min to just 18.2% ± 2.0% at 1 d.

The higher sorption affinity of Hg(II) and MMHg to Sediment 1 is consistent with the greater %LOI of that sediment. Organic matter coatings, particularly reduced sulfur groups in that organic matter, on particles enhance sorption of both Hg(II) and MMHg [53, 54] and Hg(II) and MMHg partitioning onto sediments is correlated with organic matter content [55, 56]. However, the impact of increased and faster sorption of Hg(II) on methylation is difficult to determine. Sorbed Hg(II) is generally thought to be less available for methylation than dissolved Hg(II), but there is evidence of methylation of sorbed Hg(II) [57, 58]. The same organic matter that enhances Hg(II) sorption onto the solid phase may also increase the microbial activity of Hg-methylators, masking decreases in methylation due to lower Hg(II) availability [59].

The difference in MMHg sorption between Sediment 1 and Sediment 2 was much more dramatic than for Hg(II) and has implications for the fate of MMHg in the EFPC system. Low sorption of MMHg by Sediment 2 indicates that MMHg that is produced in Sediment 2 would be readily supplied to the water column. The differences in sorption of MMHg for the two sediments could also have implications for demethylation, though it is unclear what the overall

effect might be. Lower sorption of MMHg might enhance the bioavailability of MMHg for demethylating bacteria or decrease abiotic demethylation of MMHg due to less contact with reduced sulfur surfaces.

3.3 Methylation/Demethylation Assay

3.3.1 MMHg production and biogeochemistry. In 4 days, Sediment 1 produced almost 5 times the MMHg produced by Sediment 2 in 14 days (Figure 4). The difference in MMHg production in the two sediments reflects the more conducive conditions for Hg-methylating activity in the Sediment 1 microcosms, which was richer in organic matter and anaerobic microbial activity (CH_4 production) than Sediment 2. The ancillary geochemical data from the microcosm experiments supports these findings. The initial DOC was higher in Sediment 1 microcosms compared to Sediment 2 (Figure S5), which contributed to higher microbial activity and more reducing conditions in the Sediment 1 microcosms. Microbial Hg(II) methylation occurs under anoxic conditions [5, 60]. While ample Fe(II) was generated in both Sediment 1 and Sediment 2 microcosms (Figure S6), reflecting anaerobic microbial activity, Sediment 1 microcosms showed a greater decrease in sulfate over time and generated at least 5 times more sulfide (Figure S7). This distinction is important as sulfate-reducers have been shown to have some of the greatest methylation rates [6]. Overall, the greater organic matter content, sulfide and methane production results indicate Sediment 1 was better poised for MMHg generation.

After incubation, the 16S microbial community composition remained similar to the initial community in Sediment 1 (Figure S3). Sediment 2 showed an increase in *Proteobacteria* and *Bacteroidetes* (Figure S3) and shifts in the *hgcA*-containing microbial community were more pronounced (Figure S4, Figure 3). The *hgcA* abundance showed a significant increase in *Proteobacteria* genes in Sediment 2 and a decrease in the relative abundance of methanogenic

Euryarchaeota, *Firmicutes*, and *Chloroflexi*. The relative abundance of *hgcA* genes in Sediment 1 remained more constant over the experimental timescale. The pattern of change in diversity over time also varied between the two sediment types (Figure S8). The Alpha diversity index for the 16S community generally increased over the course of the incubation for Sediment 1. Alpha diversity was initially slightly higher in Sediment 2 relative to Sediment 1 before decreasing slightly over the course of the incubation. These differences in magnitude of 16S community change between the two sediments may simply reflect the difference in incubation time between the two samples; since Sediment 1 was more metabolically active than Sediment 2 and the latter underwent a longer incubation period.

While *Deltaproteobacteria* are known to contribute to MMHg generation in stream environments including EFPC[61] and are likely contributing to the MMHg production in these microcosms, the change in relative abundance of *Deltaproteobacteria* does not appear to be a major driver behind the different rates of MMHg generation observed in these two sediments. Sediment 2 saw a marked increase in the relative abundance of both 16S and *hgcA* genes from *Desulfarculales, Desulfuromonadales*, *Desulfobacterales* and additional *Deltaproteobacterial hgcA* sequences that could not be more specifically classified (Figure 3, Figure S9). In Sediment 1, the changes in relative abundance of *Deltaproteobacterial* sequences over time were less pronounced and cannot explain the enhanced methylation rate of Sediment 1 relative to Sediment 2.

Another key difference between the 16S and *hgcA*-containing microbial communities of the two sediment types was the relative abundance of methanogenic Archaea, both overall and within the subset of the community containing the *hgcA* genes. Sediment 1 had a higher initial relative abundance of *Euryarchaeota*, including methanogens, which remained constant over the

course of the experiment and was consistent with the enhanced methane generation observed relative to Sediment 2 (Figure S10; Figure S3). Sediment 2 began with fewer *Euryarchaea* lineages overall and lost many of them by the end of the experiment. This trend is very pronounced in the *Methanomicrobiales*, a clade containing many of the known methylating species of methanogenic Archaea [62]. Their metabolic activity may contribute to the measured difference in Hg(II) methylation between the two sediment types.

3.3.2 MMHg demethylation. The overall trends in demethylation (Figure 4) were similar in both sediments with a generally stable decline of $MM^{202}Hg$ during incubations although they occurred over very different time scales. Approximately 70% of the added $MM^{202}Hg$ was lost from Sediment 1 microcosms in four days compared to 55% loss from Sediment 2 microcosms in fourteen days. The difference in demethylation rate suggests that demethylation was impacted by the relative differences in microbial activity and redox between the two sediments. Increased microbial activity could impact demethylation directly via the activity of demethylating bacteria or by driving the redox potential lower creating an environment favorable for abiotic demethylation catalyzed by reduced sulfur surfaces, such as FeS [28]. We did not directly observe FeS solid phases in these microcosms. Nevertheless, pyrite (FeS_2) has been identified by x-ray diffraction analysis in sediments collected from the same location from which Sediment 1 was collected [63]. The microcosms were in equilibrium with or oversaturated with respect to FeS solid phases throughout the incubations, indicating the potential for incipient precipitation of these solids that could catalyze the abiotic demethylation of MMHg [28, 29] (Figure S11). Additionally, the apparent lower dissolved Total Fe and Fe(II) concentrations in Sediment 1 microcosms could be explained by the precipitation of FeS solids. Although microbial activity and redox likely impacted the rate of demethylation in the microcosms, the similar overall trend in demethylation

in Sediment 1 and Sediment 2 microcosms, may indicate that demethylation was less sensitive to changes in microbial activity and redox than methylation. This could be because of the multiple pathways for demethylation (abiotic and biotic via a wider community of microorganisms) compared to the single pathway for methylation (biotic via *hgcAB*-containing microbes).

3.4.3 Transient Availability Modeling

The transient availability model (Equations 1 and 2) provided an adequate fit of Sediment 2 methylation and demethylation data and Sediment 1 demethylation data (Figure 4). The estimated demethylation rate constant (k_d) obtained by fitting the TAM to the data from Sediment 1 ($k_d = 2.23 \pm 0.24\ d^{-1}$) was approximately 25 times higher than the k_d of Sediment 2 ($(8.33 \pm 0.41) \times 10^{-2}\ d^{-1}$) (Table 2). The TAM-derived methylation rate constant for Sediment 1 ($(8.9 \pm 1.3) \times 10^{-2}\ d^{-1}$) was more than 600 times higher than the methylation rate potential for Sediment 2 ($(1.36 \pm 0.23) \times 10^{-4}\ d^{-1}$) (Table 2). However, the model did not provide an adequate fit to the methylation data in Sediment 1, over-predicting MMHg production at early time followed by an extended plateau implying a zero net rate of $MM^{201}Hg$ production at those later times (Figure 4a).

MMHg production is a function of Hg(II) availability for methylation, MMHg demethylation, and the activity of Hg-methylating microorganisms [5, 17]. The TAM accounts for changing Hg(II)/MMHg availability for methylation and demethylation reactions but does not incorporate a term to address concentration-dependent microbial activity over time.

As an initial step toward incorporating concentration-dependent microbial activity over the course of the experiment, the TAM model was modified by replacing the pseudo first-order kinetic terms for methylation and demethylation with Monod-type kinetic terms. This empirical expression has been widely applied to describe variable rate as a function of substrate

concentration. In this case, the rates of methylation and demethylation are expressed as a function of dissolved Hg(II) and MMHg concentration, respectively. To include Monod kinetics equations (1) and (2) were updated as follows:

$$(3)\quad \frac{d[Hg]}{dt} = -\frac{k_{m,\,max}[Hg]}{K_{m,\,hs} + [Hg]} + \frac{k_{d,\,max}\,[MMHg]}{K_{d,hs} + [MMHg]} - k_1[Hg] + k_2[Hg_f] - k_3[Hg] + k_4\,[Hg_s] - k_5\,[Hg] + k_6[Hg^0]$$

$$(4)\quad \frac{d[MMHg]}{dt} = \frac{k_{m,max}[Hg]}{K_{m,hs} + [Hg]} - \frac{k_{d,max}\,[MMHg]}{K_{d,hs} + [MMHg]} - k_7[MMHg] + k_8[MMHg_f] - k_9[MMHg] + k_{10}[MMHg_s]$$

Whereas the original TAM has two adjustable parameters describing methylation and demethylation (k_m and k_d), the Monod-modified TAM (TAM-M) has four fitted parameters: maximum methylation rate ($k_{m,\,max}$, M T^{-1} or M L^{-3} T^{-1}), half saturation coefficient for methylation ($K_{m,\,hs}$, M or M L^{-3}), maximum demethylation rate ($k_{d,\,max}$, M T^{-1} or M L^{-3} T^{-1}), half saturation coefficient for demethylation ($K_{d,\,hs}$, M or M L^{-3}). Because the TAM-M has more adjustable parameters than the TAM, one might expect an improved fit to the data when comparing model fits using a metric like the sum of squared errors. We used the corrected Akaike Information Criterion (*AICc*) to evaluate model fit to the data which can be used to assess the balance between model goodness-of-fit and model simplicity. The TAM-M model provided an improved fit for Sediment 1 (Figure 4, black dashed line) as indicated by a lower *AICc* which decreased from 216 for the original TAM model to 142 with the TAM-M ($k_{m,\,max}$ = 135 ng day^{-1}, $K_{m,\,hs}$ = 1.2 ng, $k_{d,\,max}$ = 96.2 ng day^{-1}, and $K_{d,\,hs}$ = 0.18 ng) (Figure 3a and 3a). The reduction in *AICc* implies the additional parameters are justified, however the parameter uncertainties were very large and a unique solution was not obtained (final parameter estimates were moderately dependent on initial estimates). Moreover, large estimated uncertainty in parameter values are strong indications that local error estimates based on small perturbations around the best-fit parameters parameter uncertainty estimates are not meaningful, which prevented evaluation of

the 95% prediction interval as was done with the TAM (Table 2). Interestingly, the TAM gave a good fit for Sediment 1 demethylation data. This could indicate that demethylation was less sensitive to the changes in microbial activity over time.

Parameter uncertainty estimates reported here are based on the covariance matrix, which are linearized estimates that are only valid for nonlinear models near the best-fit parameter values. The failure of that local uncertainty analysis in the TAM-M model is caused by high parameter uncertainty combined with significant nonlinearity in the model. Simulation-based methods that robustly search the global parameter space would provide meaningful uncertainty estimates in this situation. A potential direction for future research is to apply such global uncertainty quantification to these experiments to gain insights into parameter identifiability and model structural adequacy for the TAM-M model.

In contrast to Sediment 1, the data for Sediment 2 were reasonably well-described with the original TAM structure without including the Monod kinetics. Thus, we did not adjust the model structure to include Monod kinetics, as we did for Sediment 1. Although the methylating microbial community shifted over time in Sediment 2, those microbes may not have been very active, as overall microbial activity appeared low in Sediment 2 compared to Sediment 1 based on overall production of CO_2, CH_4, Fe^{2+} and S^{2-}. We do not have information on *hgcA* expression in our incubation experiments and whether expression changed over time. Indeed, it is unknown what environmental parameters affect the expression of the methylation genes, *hgcAB*, or how much changes in expression might impact net MMHg production. Previous studies have reported mixed results for the correlation of *hgcA* abundance with MMHg concentration [68-70], and thus far, no relationship has been observed between *hgcA* expression and MMHg concentration [68, 69, 71]. Nevertheless, these results suggest that including a measure of

concentration-dependent microbial activity can improve models of Hg(II) methylation although improvements in experiment design, model structure, and parameter estimation are needed to reduce uncertainty in parameter estimates.

4. CONCLUSION

Although the importance of microbes to MMHg production has been known for decades, this is the first attempt of which we are aware to account for concentration-dependent microbial activity in a MMHg production model. In broad terms, the TAM paradigm was applicable to these sediment incubations. Overall patterns in the data suggested a changing microbial community and *hgcA*-bearing community, and concentration-dependent microbial activity which necessitated changes to the model structure.

The TAM-M is a first step towards better estimations of MMHg production in metabolically active sediments by relating reaction rate to substrate concentration. The TAM-M is dependent on total dissolved Hg(II) and MMHg concentration. The changing geochemical conditions during the incubations also imply dynamic Hg(II) aqueous speciation (Table S7). For example, over the course of the incubations the amount of the charged aqueous species HgS_2H^- increased and the amount of the uncharged aqueous species $Hg(SH)_2$ decreased in both sediments. Our current understanding enables predictions of Hg(II) equilibrium aqueous speciation but we lack the ability to directly measure most of these species and lack the fundamental understanding of Hg(II) speciation kinetics and exactly which Hg(II) species are taken up and methylated by bacteria. Nevertheless, it is plausible that dynamic Hg(II) speciation under the changing geochemical conditions during the incubations is a contributing mechanism to the concentration-dependent activity expressed in the TAM-M.

The geochemistry data from the microcosms suggest dynamic changes in redox conditions over the course of the incubation tests, especially for Sediment 1. The changes in redox condition are indicators of broader changes to metabolic activity for the overall microbial community and would likely extend to Hg(II) methylation and demethylation, too. The changes in metabolic activity could be due to one or more limiting resources (e.g., consumption and depletion of labile organic matter[64]), product accumulation, or some combination of these factors.

Additionally, different Hg(II) methylating microbial strains produce MMHg at different rates [65] and the same strain can display different MMHg production kinetics under different culture conditions [23, 66]. Our *hgcA* sequencing data show changes in the relative abundances of the *hgcA*-containing community over the course of the incubation experiment, with more pronounced changes occurring in Sediment 2. Future improvements for quantifying *hgcA* abundance and particularly for quantifying expression may allow for future model iterations informed by targeted microbial activity or genome-level information.

The finding that different models are needed to fit MMHg production in the two different sediments is also an important result. Many ecosystems are heterogenous in regard to sediment type. With some knowledge of the relative proportion of one sediment type to another within an ecosystem, both types of models (TAM and TAM-M) could be used for more accurate reach-scale models for MMHg production.

The goal of experiments and modeling efforts like those described here is to develop the capability to predict MMHg concentrations in the environment[15]. Future advances in this effort will be greatly aided by coupling our models of methylation and demethylation with reactive transport codes that include aqueous speciation, sorption, mineral equilibria, etc. to make the

models chemically aware. Improved understanding of exactly which Hg(II) species are recognized and methylated by bacteria, including the mechanisms and kinetics of Hg(II) exchange and uptake, will be critical to take full advantage of this capability. Such models will also be enhanced with better thermodynamic data relevant to Hg(II) nanoparticle behavior [19]. Advances in microbial ecology and molecular techniques will also be invaluable as we seek to develop relationships between *hgcA* presence, its expression, and MMHg production and how those processes depend on the relationship of *hgcA*-carrying microorganisms within their broader and more complex communities within the context of real geochemical systems.

DATA AVAILABILITY STATEMENT

The data presented in the paper and supporting information are publicly available at https://msfa.ornl.gov/data/pages/MCI546.html. For additional information please contact the corresponding author. The sequence reads for the 16S and *hgcA* amplicons have been deposited in NCBI SRA repository under the accession numbers SRR14845146-SRR14845153 and SRR15334643-SRR15334650, respectively, and are publicly available at https://www.ncbi.nlm.nih.gov/Traces/study/?acc=PRJNA738663

Acknowledgement

We thank Kenneth Lowe, Emily Angell, and Jada Hoyle-Gardner for their assistance with field sampling and laboratory analyses and Julia Brenner for her assistance with the gas production measurements. The isotopes used in this research were supplied by the United States Department of Energy Office of Science by the Isotope Program in the Office of Nuclear Physics. This work was funded by the U.S. Department of Energy, Office of Science, Biological and Environmental Research, Subsurface Biogeochemical Research (SBR) Program, and is a

product of the Science Focus Area at Oak Ridge National Laboratory. Oak Ridge National Laboratory is managed by UT-Battelle, LLC, for the U.S. Department of Energy under contract DE-AC05-00OR22725.

References

1. C. S. Eckley, C. C. Gilmour, S. Janssen, T. P. Luxton, P. M. Randall, L. Whalin and C. Austin, The assessment and remediation of mercury contaminated sites: A review of current approaches, *Science of The Total Environment*, 2020, **707**, 136031.

2. T. W. Clarkson, L. Magos and G. J. Myers, The Toxicology of Mercury — Current Exposures and Clinical Manifestations, *New England Journal of Medicine*, 2003, **349**, 1731-1737.

3. D. Mergler, H. A. Anderson, L. H. M. Chan, K. R. Mahaffey, M. Murray, M. Sakamoto and A. H. Stern, Methylmercury Exposure and Health Effects in Humans: A Worldwide Concern, *AMBIO: A Journal of the Human Environment*, 2007, **36**, 3-11, 19.

4. J. M. Parks, A. Johs, M. Podar, R. Bridou, R. A. Hurt, S. D. Smith, S. J. Tomanicek, Y. Qian, S. D. Brown, C. C. Brandt, A. V. Palumbo, J. C. Smith, J. D. Wall, D. A. Elias and L. Liang, The Genetic Basis for Bacterial Mercury Methylation, *Science*, 2013, **339**, 1332.

5. A. G. Bravo and C. Cosio, Biotic formation of methylmercury: A bio–physico–chemical conundrum, *Limnology and Oceanography*, 2019, **9999**, 1-18.

6. C. C. Gilmour, M. Podar, A. L. Bullock, A. M. Graham, S. D. Brown, A. C. Somenahally, A. Johs, R. A. Hurt, K. L. Bailey and D. A. Elias, Mercury Methylation by Novel Microorganisms from New Environments, *Environmental Science & Technology*, 2013, **47**, 11810-11820.

7. M. Podar, C. C. Gilmour, C. C. Brandt, A. Soren, S. D. Brown, B. R. Crable, A. V. Palumbo, A. C. Somenahally and D. A. Elias, Global prevalence and distribution of genes and microorganisms involved in mercury methylation, *Sci Adv*, 2015, **1**, e1500675.

8. H. Hintelmann, K. Keppel-Jones and R. D. Evans, Constants of mercury methylation and demethylation rates in sediments and comparison of tracer and ambient mercury availability, *Environ. Toxicol. Chem.*, 2000, **19**, 2204-2211.

9. H. Hintelmann, K. Keppel-Jones and R. D. Evans, Constants of mercury methylation and demethylation rates in sediments and comparison of tracer and ambient mercury availability, *Environmental Toxicology and Chemistry*, 2000, **19**, 2204-2211.

10. C. P. J. Mitchell and C. C. Gilmour, Methylmercury production in a Chesapeake Bay salt marsh, *Journal of Geophysical Research: Biogeosciences*, 2008, **113**.

11. R. C. Rodríguez Martín-Doimeadios, E. Tessier, D. Amouroux, R. Guyoneaud, R. Duran, P. Caumette and O. F. X. Donard, Mercury methylation/demethylation and volatilization pathways in estuarine sediment slurries using species-specific enriched stable isotopes, *Marine Chemistry*, 2004, **90**, 107-123.

12. V. Liem-Nguyen, S. Jonsson, U. Skyllberg, M. B. Nilsson, A. Andersson, E. Lundberg and E. Björn, Effects of Nutrient Loading and Mercury Chemical Speciation on the Formation and Degradation of Methylmercury in Estuarine Sediment, *Environmental Science & Technology*, 2016, **50**, 6983-6990.

13. S. Jonsson, U. Skyllberg, M. B. Nilsson, P. O. Westlund, A. Shchukarev, E. Lundberg and E. Björn, Mercury methylation rates for geochemically relevant Hg(II) species in sediments, *Environ Sci Technol*, 2012, **46**, 11653-11659.

14. M.-L. Avramescu, E. Yumvihoze, H. Hintelmann, J. Ridal, D. Fortin and D. R.S. Lean, Biogeochemical factors influencing net mercury methylation in contaminated freshwater sediments from the St. Lawrence River in Cornwall, Ontario, Canada, *Science of The Total Environment*, 2011, **409**, 968-978.

15. T. A. Olsen, K. A. Muller, S. L. Painter and S. C. Brooks, Kinetics of Methylmercury Production Revisited, *Environmental Science & Technology*, 2018, **52**, 2063-2070.

16. G. E. Schwartz, T. A. Olsen, K. A. Muller and S. C. Brooks, Ecosystem Controls on Methylmercury Production by Periphyton Biofilms in a Contaminated Stream: Implications for Predictive Modeling, *Environmental Toxicology and Chemistry*, 2019, **38**, 2426-2435.

17. K. H. Kucharzyk, M. A. Deshusses, K. A. Porter and H. Hsu-Kim, Relative contributions of mercury bioavailability and microbial growth rate on net methylmercury production by anaerobic mixed cultures, *Environmental Science: Processes & Impacts*, 2015, **17**, 1568-1577.

18. G. A. Christensen, A. C. Somenahally, J. G. Moberly, C. M. Miller, A. J. King, C. C. Gilmour, S. D. Brown, M. Podar, C. C. Brandt, S. C. Brooks, A. V. Palumbo, J. D. Wall and D. A. Elias, Carbon Amendments Alter Microbial Community Structure and Net Mercury Methylation Potential in Sediments, *Appl Environ Microbiol*, 2018, **84**.

19. H. Hsu-Kim, K. H. Kucharzyk, T. Zhang and M. A. Deshusses, Mechanisms regulating mercury bioavailability for methylating microorganisms in the aquatic environment: a critical review, *Environ Sci Technol*, 2013, **47**, 2441-2456.

20. S. Åkerblom, M. B. Nilsson, U. Skyllberg, E. Björn, S. Jonsson, B. Ranneby and K. Bishop, Formation and mobilization of methylmercury across natural and experimental sulfur deposition gradients, *Environmental Pollution*, 2020, **263**, 114398.

21. J. S. Waples, K. L. Nagy, G. R. Aiken and J. N. Ryan, Dissolution of cinnabar (HgS) in the presence of natural organic matter, *Geochimica et Cosmochimica Acta*, 2005, **69**, 1575-1588.

22. M. Ravichandran, G. R. Aiken, J. N. Ryan and M. M. Reddy, Inhibition of Precipitation and Aggregation of Metacinnabar (Mercuric Sulfide) by Dissolved Organic Matter Isolated from the Florida Everglades, *Environmental Science & Technology*, 1999, **33**, 1418-1423.

23. A. M. Graham, G. R. Aiken and C. C. Gilmour, Dissolved Organic Matter Enhances Microbial Mercury Methylation Under Sulfidic Conditions, *Environmental Science & Technology*, 2012, **46**, 2715-2723.

24. A. M. Graham, G. R. Aiken and C. C. Gilmour, Effect of Dissolved Organic Matter Source and Character on Microbial Hg Methylation in Hg–S–DOM Solutions, *Environmental Science & Technology*, 2013, **47**, 5746-5754.

25. G. R. Aiken, H. Hsu-Kim and J. N. Ryan, Influence of Dissolved Organic Matter on the Environmental Fate of Metals, Nanoparticles, and Colloids, *Environmental Science & Technology*, 2011, **45**, 3196-3201.

26. A. M. Graham, K. T. Cameron-Burr, H. A. Hajic, C. Lee, D. Msekela and C. C. Gilmour, Sulfurization of Dissolved Organic Matter Increases Hg–Sulfide–Dissolved Organic Matter Bioavailability to a Hg-Methylating Bacterium, *Environmental Science & Technology*, 2017, **51**, 9080-9088.

27. C. Gilmour, J. T. Bell, A. B. Soren, G. Riedel, G. Riedel, A. D. Kopec and R. A. Bodaly, Distribution and biogeochemical controls on net methylmercury production in Penobscot River marshes and sediment, *Science of The Total Environment*, 2018, **640-641**, 555-569.

28. S. Jonsson, N. M. Mazrui and R. P. Mason, Dimethylmercury Formation Mediated by Inorganic and Organic Reduced Sulfur Surfaces, *Scientific Reports*, 2016, **6**, 27958.

29. J. West, A. M. Graham, V. Liem-Nguyen and S. Jonsson, Dimethylmercury Degradation by Dissolved Sulfide and Mackinawite, *Environmental Science & Technology*, 2020, **54**, 13731-13738.

30. S. C. Brooks and G. R. Southworth, History of mercury use and environmental contamination at the Oak Ridge Y-12 Plant, *Environmental Pollution*, 2011, **159**, 219-228.

31. A. Riscassi, C. Miller and S. Brooks, Seasonal and flow-driven dynamics of particulate and dissolved mercury and methylmercury in a stream impacted by an industrial mercury source, *Environmental Toxicology and Chemistry*, 2016, **35**, 1386-1400.

32. C. Bancon-Montigny, L. Yang, R. E. Sturgeon, V. Colombini and Z. Mester, High-yield synthesis of milligram amounts of isotopically enriched methylmercury (CH3198HgCl), *Applied Organometallic Chemistry*, 2004, **18**, 57-64.

33. L. S. Clesceri, A. D. Eaton, M. A. H. Franson and A. E. Greenberg, *Standard methods for the examination of water and wastewater*, American Public Health Association, Washington, DC, 20th edn edn., 1998.

34. L. L. Stookey, Ferrozine---a new spectrophotometric reagent for iron, *Analytical Chemistry*, 1970, **42**, 779-781.

35. N. S. Bloom, J. A. Colman and L. Barber, Artifact formation of methyl mercury during aqueous distillation and alternative techniques for the extraction of methyl mercury from environmental samples, *Fresenius' Journal of Analytical Chemistry*, 1997, **358**, 371-377.

36. US EPA, *US EPA Method 1630: Methyl mercury in water by distillation, aqueous ethylaton, purge and trap, and cold vapor atomic fluorescence spectroscopy*, United States Environmental Protection Agency, Washington, D.C., 2001.

37. US EPA, *US EPA Method 1631, Revision D: Mercury in Water by Oxidation, Purge, and Trap, 526 and Cold Vapor Atomic Fluorescence Spectroscopy*, U.S. EPA, Washington, D.C., 2001.

38. D. S. Lundberg, S. Yourstone, P. Mieczkowski, C. D. Jones and J. L. Dangl, Practical innovations for high-throughput amplicon sequencing, *Nat Methods*, 2013, **10**, 999-1002.

39. X. Liang, J. M. Whitham, E. K. Holwerda, X. Shao, L. Tian, Y. W. Wu, V. Lombard, B. Henrissat, D. M. Klingeman, Z. K. Yang, M. Podar, T. L. Richard, J. G. Elkins, S. D. Brown and L. R. Lynd, Development and characterization of stable anaerobic thermophilic methanogenic microbiomes fermenting switchgrass at decreasing residence times, *Biotechnol Biofuels*, 2018, **11**, 243.

40. C. M. Gionfriddo, A. M. Wymore, D. S. Jones, R. L. Wilpiszeski, M. M. Lynes, G. A. Christensen, A. Soren, C. C. Gilmour, M. Podar and D. A. Elias, An Improved *hgcAB* Primer Set and Direct High-Throughput Sequencing Expand Hg-Methylator Diversity in Nature, *Front Microbiol*, 2020, **11**, 541554.

41. E. Bolyen, J. R. Rideout, M. R. Dillon, N. A. Bokulich, C. C. Abnet, G. A. Al-Ghalith, H. Alexander, E. J. Alm, M. Arumugam, F. Asnicar, Y. Bai, J. E. Bisanz, K. Bittinger, A. Brejnrod, C. J. Brislawn, C. T. Brown, B. J. Callahan, A. M. Caraballo-Rodríguez, J. Chase, E. K. Cope, R. Da Silva, C. Diener, P. C. Dorrestein, G. M. Douglas, D. M. Durall, C. Duvallet, C. F. Edwardson, M. Ernst, M. Estaki, J. Fouquier, J. M. Gauglitz, S. M. Gibbons, D. L. Gibson, A. Gonzalez, K. Gorlick, J. Guo, B. Hillmann, S. Holmes, H. Holste, C. Huttenhower, G. A. Huttley, S. Janssen, A. K. Jarmusch, L. Jiang, B. D. Kaehler, K. B. Kang, C. R. Keefe, P. Keim, S. T. Kelley, D. Knights, I. Koester, T. Kosciolek, J. Kreps, M. G. I. Langille, J. Lee, R. Ley, Y. X. Liu, E. Loftfield, C. Lozupone, M. Maher, C. Marotz, B. D. Martin, D. McDonald, L. J. McIver, A. V. Melnik, J. L. Metcalf, S. C. Morgan, J. T. Morton, A. T. Naimey, J. A. Navas-Molina, L. F. Nothias, S. B. Orchanian, T. Pearson, S. L. Peoples, D. Petras, M. L. Preuss, E. Pruesse, L. B. Rasmussen, A. Rivers, M. S. Robeson, P. Rosenthal, N. Segata, M. Shaffer, A. Shiffer, R. Sinha, S. J. Song, J. R. Spear, A. D. Swafford, L. R. Thompson, P. J. Torres, P. Trinh, A. Tripathi, P. J. Turnbaugh, S. Ul-Hasan, J. J. J. van der Hooft, F. Vargas, Y. Vázquez-Baeza, E. Vogtmann, M. von Hippel, W. Walters, Y. Wan, M. Wang, J. Warren, K. C. Weber, C. H. D. Williamson, A. D. Willis, Z. Z. Xu, J. R. Zaneveld, Y. Zhang, Q. Zhu, R. Knight and J. G. Caporaso, Reproducible, interactive,

scalable and extensible microbiome data science using QIIME 2, *Nat Biotechnol*, 2019, **37**, 852-857.

42. B. J. Callahan, P. J. McMurdie, M. J. Rosen, A. W. Han, A. J. Johnson and S. P. Holmes, DADA2: High-resolution sample inference from Illumina amplicon data, *Nat Methods*, 2016, **13**, 581-583.

43. C. Quast, E. Pruesse, P. Yilmaz, J. Gerken, T. Schweer, P. Yarza, J. Peplies and F. O. Glöckner, The SILVA ribosomal RNA gene database project: improved data processing and web-based tools, *Nucleic Acids Res*, 2013, **41**, D590-596.

44. N. A. Bokulich, B. D. Kaehler, J. R. Rideout, M. Dillon, E. Bolyen, R. Knight, G. A. Huttley and J. Gregory Caporaso, Optimizing taxonomic classification of marker-gene amplicon sequences with QIIME 2's q2-feature-classifier plugin, *Microbiome*, 2018, **6**, 90.

45. A. M. Bolger, M. Lohse and B. Usadel, Trimmomatic: a flexible trimmer for Illumina sequence data, *Bioinformatics*, 2014, **30**, 2114-2120.

46. R. C. Edgar, Search and clustering orders of magnitude faster than BLAST, *Bioinformatics*, 2010, **26**, 2460-2461.

47. C. Gionfriddo, M. Podar, C. Gilmour, E. Pierce and D. Elias, ORNL Compiled Mercury Methylator Database.*Journal*, 2019, DOI: 10.12769/1569274.

48. P. J. McMurdie and S. Holmes, phyloseq: an R package for reproducible interactive analysis and graphics of microbiome census data, *PLoS One*, 2013, **8**, e61217.

49. H. Wickham, ggplot2, *WIREs Computational Statistics*, 2011, **3**, 180-185.

50. T. A. Vishnivetskaya, J. J. Mosher, A. V. Palumbo, Z. K. Yang, M. Podar, S. D. Brown, S. C. Brooks, B. Gu, G. R. Southworth, M. M. Drake, C. C. Brandt and D. A. Elias, Mercury and other heavy metals influence bacterial community structure in contaminated Tennessee streams, *Appl Environ Microbiol*, 2011, **77**, 302-311.

51. S. Painter, V. Cvetkovic, D. Pickett and D. R. Turner, Significance of Kinetics for Sorption on Inorganic Colloids: Modeling and Experiment Interpretation Issues, *Environmental Science & Technology*, 2002, **36**, 5369-5375.

52. Y.-J. Kim, S. C. Brooks, F. Zhang, J. C. Parker, J.-W. Moon and Y. Roh, Fate and transport of uranium (VI) in weathered saprolite, *Journal of Environmental Radioactivity*, 2015, **139**, 154-162.

53. C. Gagnon and N. S. Fisher, Bioavailability of Sediment-Bound Methyl and Inorganic Mercury to a Marine Bivalve, *Environmental Science & Technology*, 1997, **31**, 993-998.

54. L. Zhao, Y. Li, L. Zhang, J. Zheng, E. M. Pierce and B. Gu, Mercury Adsorption on Minerals and Its Effect on Microbial Methylation, *ACS Earth and Space Chemistry*, 2019, **3**, 1338-1345.

55. A. T. Schartup, R. P. Mason, P. H. Balcom, T. A. Hollweg and C. Y. Chen, Methylmercury Production in Estuarine Sediments: Role of Organic Matter, *Environmental Science & Technology*, 2013, **47**, 695-700.

56. C. R. Hammerschmidt, W. F. Fitzgerald, P. H. Balcom and P. T. Visscher, Organic matter and sulfide inhibit methylmercury production in sediments of New York/New Jersey Harbor, *Marine Chemistry*, 2008, **109**, 165-182.

57. L. Zhang, S. Wu, L. Zhao, X. Lu, E. M. Pierce and B. Gu, Mercury Sorption and Desorption on Organo-Mineral Particulates as a Source for Microbial Methylation, *Environmental Science & Technology*, 2019, **53**, 2426-2433.

58. K. A. Muller and S. C. Brooks, Effectiveness of Sorbents to Reduce Mercury Methylation, *Environmental Engineering Science*, 2019, **36**, 361-371.

59. N. M. Mazrui, S. Jonsson, S. Thota, J. Zhao and R. P. Mason, Enhanced availability of mercury bound to dissolved organic matter for methylation in marine sediments, *Geochimica et Cosmochimica Acta*, 2016, **194**, 153-162.

60. B. A. Branfireun, C. Cosio, A. J. Poulain, G. Riise and A. G. Bravo, Mercury cycling in freshwater systems - An updated conceptual model, *Sci Total Environ*, 2020, **745**, 140906.

61. J. J. Mosher, T. A. Vishnivetskaya, D. A. Elias, M. Podar, S. C. Brooks, S. D. Brown, C. C. Brandt and A. V. Palumbo, Characterization of the Deltaproteobacteria in contaminated and uncontaminated stream sediments and identification of potential mercury methylators, *Aquatic Microbial Ecology*, 2012, **66**, 271-282.

62. C. C. Gilmour, A. L. Bullock, A. McBurney, M. Podar and D. A. Elias, Robust Mercury Methylation across Diverse Methanogenic Archaea, *mBio*, 2018, **9**.

63. J. S. Yan, Neha Flynn, Elaine D. Giammar, Daniel E. Schwartz, Grace E. Brooks, Scott C. Weisenhorn, P. Kemner Kenneth M. O'Loughlin, Edward J. Kaplan, Daniel I. Catalano, Jeffrey G., Consistent Controls on Trace Metal Micronutrient Speciation in Wetland Soils and Stream Sediments, *Geochim. Cosmochim. Acta*, 2021.

64. M. Kim, S. Han, J. Gieskes and D. D. Deheyn, Importance of organic matter lability for monomethylmercury production in sulfate-rich marine sediments, *Sci Total Environ*, 2011, **409**, 778-784.

65. C. C. Gilmour, M. Podar, A. L. Bullock, A. M. Graham, S. D. Brown, A. C. Somenahally, A. Johs, R. A. Hurt, K. L. Bailey and D. A. Elias, Mercury methylation by novel microorganisms from new environments, *Environ Sci Technol*, 2013, **47**, 11810-11820.

66. C. C. Gilmour, D. A. Elias, A. M. Kucken, S. D. Brown, A. V. Palumbo, C. W. Schadt and J. D. Wall, Sulfate-reducing bacterium Desulfovibrio desulfuricans ND132 as a model for understanding bacterial mercury methylation, *Appl Environ Microbiol*, 2011, **77**, 3938-3951.

67. S. Jonsson, U. Skyllberg, M. B. Nilsson, E. Lundberg, A. Andersson and E. Björn, Differentiated availability of geochemical mercury pools controls methylmercury levels in estuarine sediment and biota, *Nat Commun*, 2014, **5**, 4624.

68. G. A. Christensen, C. M. Gionfriddo, A. J. King, J. G. Moberly, C. L. Miller, A. C. Somenahally, S. J. Callister, H. Brewer, M. Podar, S. D. Brown, A. V. Palumbo, C. C. Brandt, A. M. Wymore, S. C. Brooks, C. Hwang, M. W. Fields, J. D. Wall, C. C. Gilmour and D. A. Elias, Determining the Reliability of Measuring Mercury Cycling Gene Abundance with Correlations with Mercury and Methylmercury Concentrations, *Environmental Science & Technology*, 2019, **53**, 8649-8663.

69. A. G. Bravo, J.-L. Loizeau, P. Dranguet, S. Makri, E. Björn, V. G. Ungureanu, V. I. Slaveykova and C. Cosio, Persistent Hg contamination and occurrence of Hg-methylating transcript (hgcA) downstream of a chlor-alkali plant in the Olt River (Romania), *Environmental Science and Pollution Research*, 2016, **23**, 10529-10541.

70. T. A. Vishnivetskaya, H. Hu, J. D. Van Nostrand, Ann M. Wymore, X. Xu, G. Qiu, X. Feng, J. Zhou, S. D. Brown, C. C. Brandt, M. Podar, B. Gu and D. A. Elias, Microbial community structure with trends in methylation gene diversity and abundance in mercury-contaminated rice paddy soils in Guizhou, China, *Environmental Science: Processes & Impacts*, 2018, **20**, 673-685.

71. M. Goñi-Urriza, Y. Corsellis, L. Lanceleur, E. Tessier, J. Gury, M. Monperrus and R. Guyoneaud, Relationships between bacterial energetic metabolism, mercury methylation potential, and hgcA/hgcB gene expression in Desulfovibrio dechloroacetivorans BerOc1, *Environmental Science and Pollution Research*, 2015, **22**, 13764-13771.

Table 1. East Fork Poplar Creek Sediment Characteristics

Sediment	Major grain size fraction	Bulk sediment surface Area $m^2\ g^{-1}$	[a]Surface Area of 0.5 mm > 0.149 mm Fraction $m^2\ g^{-1}$	%LOI	Acid extractable Tot Fe, mg gdw^{-1}	Acid-extractable Fe(II), mg gdw^{-1}	TotHg, µg gdw^{-1}	MMHg, ng gdw^{-1}
Sediment 1	Fine Sand	7.752	6.836	6.97	5.79	5.66	7.5	8.44
Sediment 2	Medium Sand	5.508	2.405	1.41	0.926	0.556	14.7	1.46

[a] Size fraction used for the adsorption experiments

Table 2. Estimated parameter values and their standard errors obtained by fitting the transient availability model to the observed data

		Sediment 1		Sediment 2	
Parameter	**units**	**Value**	**SE[a]**	**Value**	**SE**
k_1	d^{-1}	370	131	513	54
k_2	d^{-1}	711	275	1908	184
k_3	d^{-1}	4.67	0.62	3.38	0.38
k_4	d^{-1}	0.21	0.20	2.61	0.39
k_5	d^{-1}	160	22	1.02	0.42
k_6	d^{-1}	7327	930	5.79	2.89
k_7	d^{-1}	58.26	7.10	491.66	89.11
k_8	d^{-1}	84.99	14.59	6974.47	588.23
k_9	d^{-1}	7.26	0.78	0.36	0.15
k_{10}	d^{-1}	1.26	0.24	1.33	1.01
k_m	d^{-1}	0.089	0.013	0.000136	0.000023
k_d	d^{-1}	2.23	0.24	0.0833	0.0041
[b]$k_{m,\,max}$	ng d^{-1}	135	3785		
[b]$K_{m,\,hs}$	ng	1.2	55.9		
[b]$k_{d,\,max}$	ng d^{-1}	96	3814		
[b]$K_{d,\,hs}$	ng	0.19	7.84		

[a] standard error
[b] parameters included in the Monod-modified TAM (TAM-M) which provided an improved fit only to Sediment 1

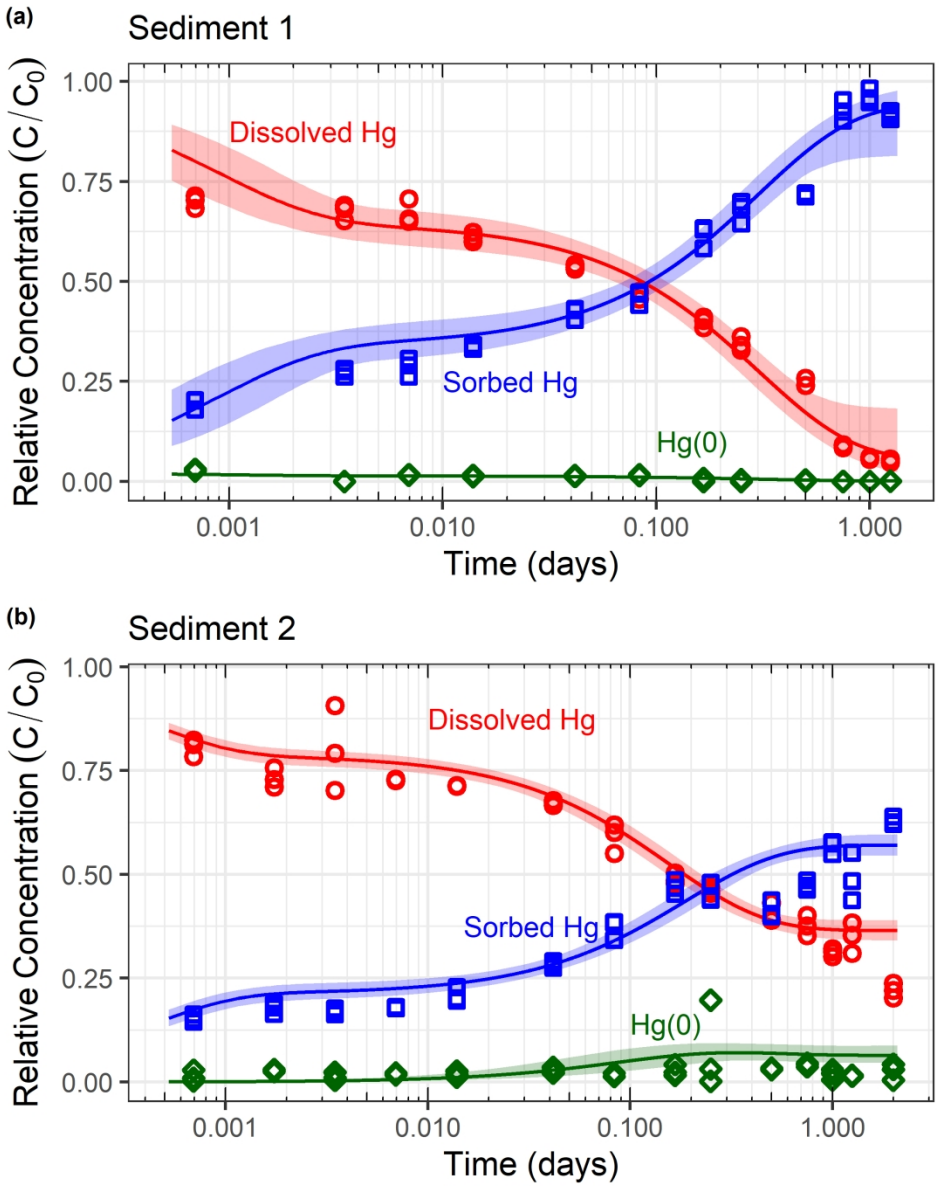

Figure 1. ^{201}Hg sorption and ^{201}Hg(0) production over time in (a) Sediment 1 (538 ng ^{201}Hg spiked), and (b) Sediment 2 (1049 ng ^{201}Hg spiked). Fraction of the total added ^{201}Hg as dissolved Hg (circles), sorbed Hg (squares), and Hg(0) (diamonds). Each symbol represents one replicate. Lines correspond to the model fit to the data, and the shaded bands are the 95% confidence intervals determined from Monte Carlo analysis (N = 5000).

516x645mm (126 x 126 DPI)

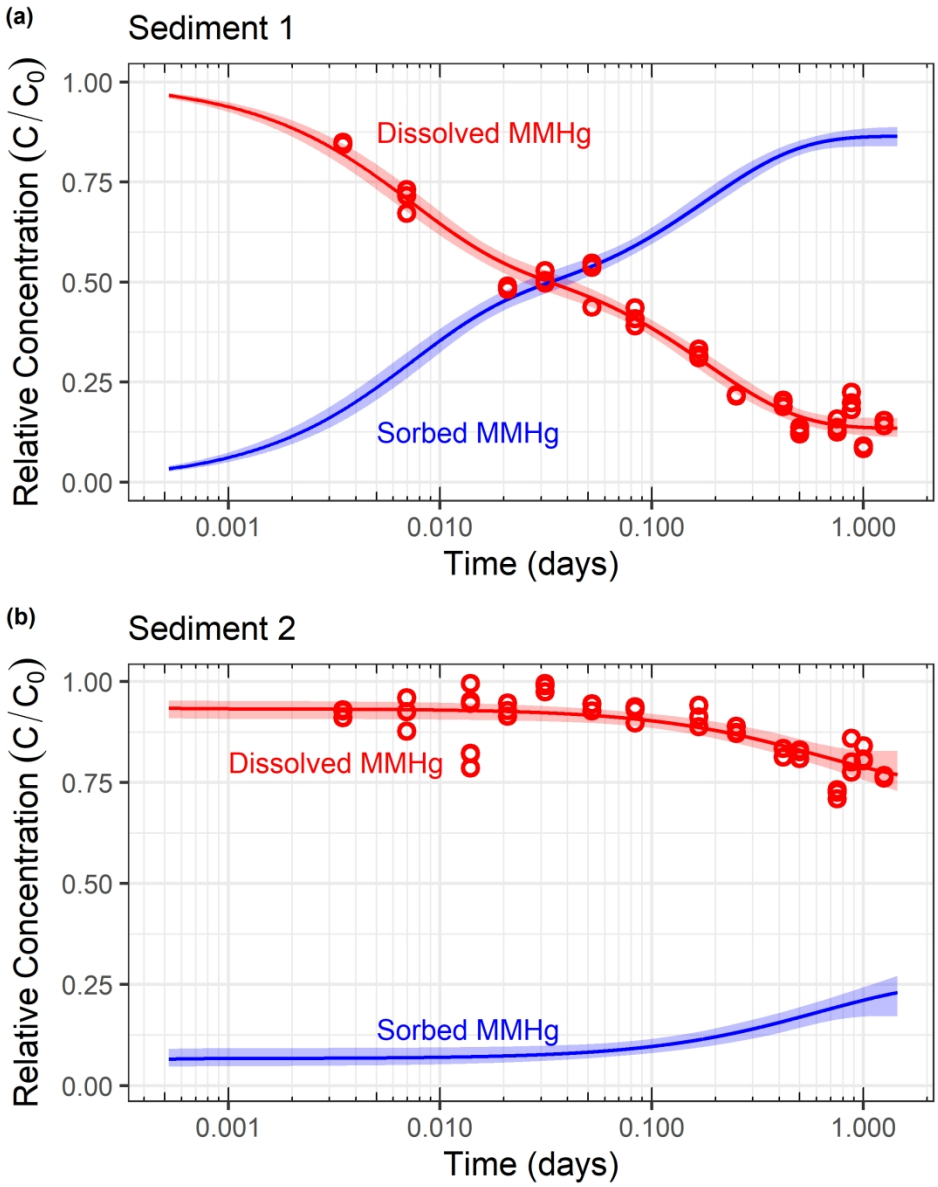

Figure 2. $MM^{202}Hg$ sorption over time in (a) Sediment 1 (4.08 ng $MM^{202}Hg$ spiked), and (b) Sediment 2 (0.680 ng $MM^{202}Hg$ spiked). Fraction of the total added $MM^{202}Hg$ as dissolved MMHg (circles). Each circle represents one replicate. Lines correspond to the model fit to the data, and the shaded bands are the 95% confidence intervals determined from Monte Carlo analysis (N = 5000).

516x645mm (126 x 126 DPI)

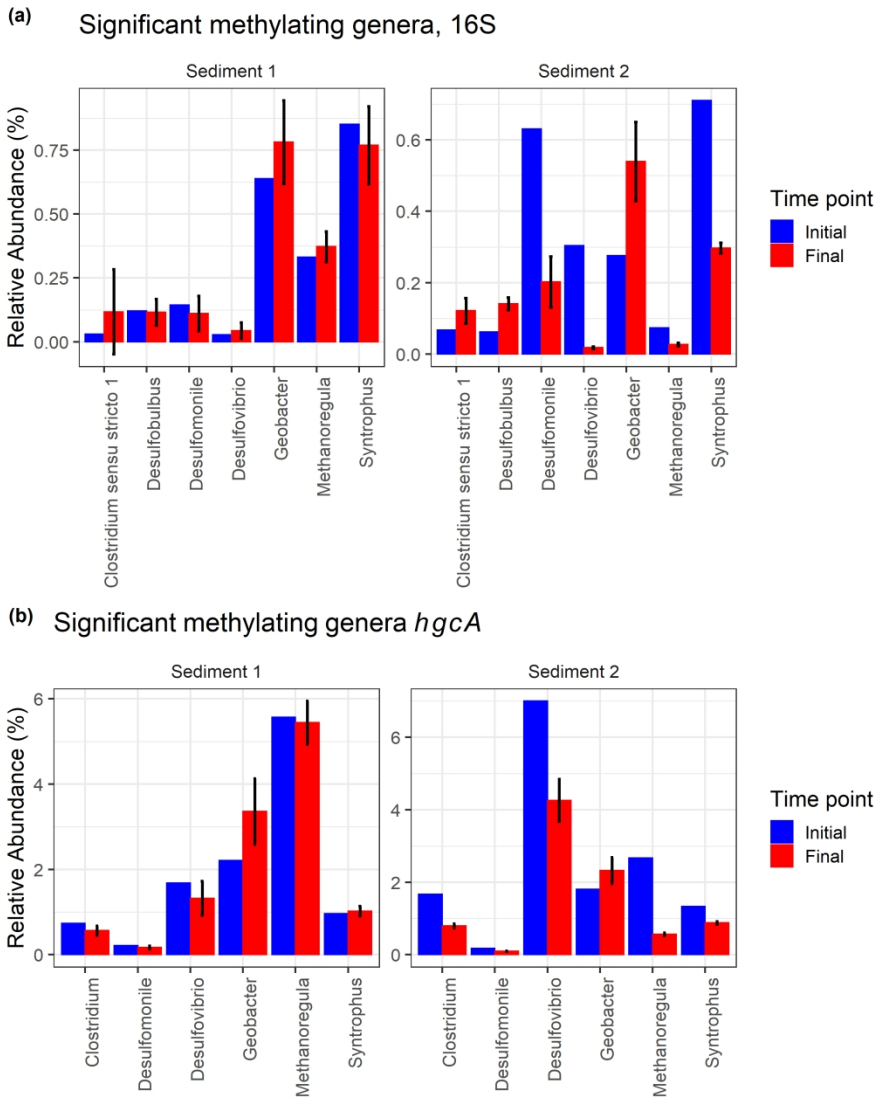

Figure 3. (a) Significant methylating genera 16S relative abundance and, (b) significant *hgcA*-containing genera relative abundance for the native Sediment 1 and 2 and respective incubation endpoints. Red bars are the average of replicate microcosms (n = 3 for Sediment 1, n = 2 for Sediment 2). Error bars represent one standard deviation.

580x774mm (126 x 126 DPI)

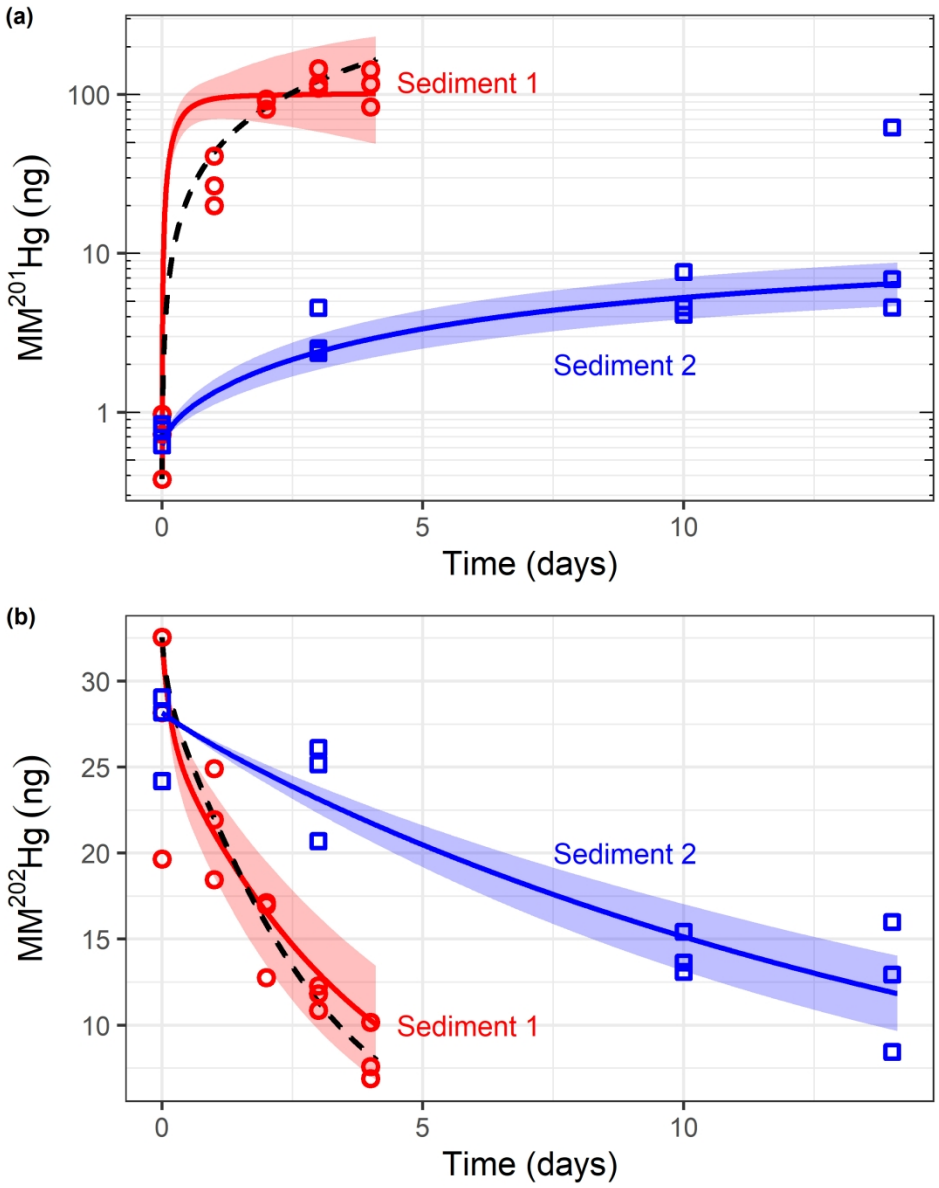

Figure 4. (a) Production of $MM^{201}Hg$ and (b) loss of $MM^{202}Hg$ over time in microcosm experiments with Sediments 1 (open circles) and 2 (open squares). The lines and ribbons indicate the TAM model fit to the data and Monte Carlo estimated 95% confidence intervals (n = 5000). The dashed black line represents the Monod modified TAM (TAM-M) fit to Sediment 1 data. Sediment 1: ^{201}Hg spiked at 6.55 µg, $MM^{202}Hg$ spiked at 28.0 ng. Sediment 2: ^{201}Hg spiked at 13.1 µg, $MM^{202}Hg$ spiked at 28.0 ng.

516x645mm (126 x 126 DPI)